Additive Manufacturing xxx (2016) xxx–xxx

Contents lists available at ScienceDirect

Additive Manufacturing

journal homepage: www.elsevier.com/locate/addma

Full Length Article

Modeling of nanoparticle agglomeration and powder bed formation in microscale selective laser sintering systems

Anil Yuksel[a,b], Michael Cullinan[a,*]

[a] Department of Mechanical Engineering University of Texas at Austin,United States
[b] NXP Inc., 6501 W William Cannon Dr. Austin, TX 78735, United States

ARTICLE INFO

Article history:
Received 5 January 2016
Received in revised form 15 June 2016
Accepted 11 July 2016
Available online xxx

Keywords:
Additive manufacturing
Selective laser sintering
Nanoparticle
Van der waals forces
Agglomeration

ABSTRACT

Additive manufacturing (AM) has received a great deal of attention for the ability to produce three dimensional parts via laser heating. One recently proposed method of making microscale AM parts is through microscale selective laser sintering (μ-SLS) where nanoparticles replace the traditional powders used in standard SLS processes. However, there are many challenges to understanding the physics of the process at nanoscale as well as with conducting experiments at that scale; hence, modeling and computational simulations are vital to understand the sintering process physics. At the sub-micron (μm) level, the interaction between nanoparticles under high power laser heating raises additional near-field thermal issues such as thermal diffusivity, effective absorptivity, and extinction coefficients compared to larger scales. Thus, nanoparticle's distribution behavior and characteristic properties are very important to understanding the thermal analysis of nanoparticles in a μ-SLS process. This paper presents a discrete element modeling (DEM) study of how copper nanoparticles of given particle size distribution pack together in a μ-SLS powder bed. Initially, nanoparticles are distributed randomly into the bed domain with a random initial velocity vector and set boundary conditions. The particles are then allowed to move in discrete time steps until they reach a final steady state position, which creates the particle packing within the powder bed. The particles are subject to both gravitational and cohesive forces since cohesive forces become important at the nanoscale. A set of simulations was performed for different cases under both Gaussian and log-normal particle size distributions with different standard deviations. The results show that the cohesive interactions between nanoparticles has a great effect on both the size of the agglomerates and how densely the nanoparticles pack together within the agglomerates. In addition, this paper suggests a potential method to overcome the agglomeration effects in μ-SLS powder beds through the use of colloidal nanoparticle solutions that minimize the cohesive interactions between individual nanoparticles.

1. Introduction

Harnessing heat transfer at the nanoscale is essential for the development of microchips in semiconductors, micro/nanoelectronics, integrated circuits, and micro/nano electromechanical systems (MEM/NEMS) [1]. Today, using nanomaterials such as nanowires, carbon nanotubes, graphene, and metal nanoparticles is common in these types of systems. Nanomaterials are generally used in these systems because the thermal, optical, and electromechanical properties of nanomaterials are quite different from the properties of the bulk material and can be tuned by controlling the shape and size of the nanostructure [1]. The key fields where nanomaterials have recently been used in additive manufacturing technologies are microscale selective laser sintering (μ-SLS), three-dimensional (3D) printing, and stereolithography [2]. μ-SLS is a relatively new additive manufacturing technique in which the structures or objects are fabricated from the bottom up by adding materials layer upon layer [3]. In this technique, a laser that has been focused down to approximately 1 μm is used to sinter together nanoparticles in a designed pattern on each layer before the next layer of nanoparticles is added to the system. This process is then repeated until an entire 3D structure with microscale features is fabricated. Through the use of precise focusing objectives, ultrafast lasers, and nanoparticle based powder beds it is possible to achieve micron scale feature resolutions with this technique.

* Corresponding author.
E-mail address: Michael.Cullinan@austin.utexas.edu (M. Cullinan).

http://dx.doi.org/10.1016/j.addma.2016.07.002
2214-8604/

μ-SLS has many advantages over other manufacturing techniques in terms of the flexibility, cost, and finishing quality. Furthermore, μ-SLS provides design freedom and has a lower level of waste and harmful chemicals. Using nanoparticles which can be synthesized with different shapes such as rods or spheres for microscale selective laser sintering can also significantly improve the sintering characteristics and the finishing quality of the parts [2]. However, models for nanoparticle interactions and powder bed generation with nanoparticles are not available for SLS at nanoscale. This is because nanoscale modeling offers many challenges; for instance, a continuum model which is used for micro and larger scales is no longer valid. Also, a ray tracing model cannot be used to obtain the extinction and effective absorption coefficient of a powder bed as the laser wavelength is greater than the characteristic length of the particles [4,5]. Hence, modeling the nanoscale powder bed with nanoparticles for SLS is quite different from modeling micro or larger scales. For example, cohesive forces, which are the sum of the attractive or repulsive intermolecular attractions between molecules, dominate interactions between the particles at nanoscale [6,7]. These cohesive interactions can create significant agglomeration effects in particle beds containing nanoscale powders which are not typically seen in SLS powder beds that contain only microscale powders. These agglomeration effects can significantly reduce the packing density of the particles in the powder bed which can result in significant voids in the final sintered part. Additionally, particle size distribution is another factor affecting the sintering process at the submicron level [8]. Most powder beds with nanoparticles have non-uniform size distributions which effect the sintering quality and overall shrinking of the parts produced. Hence, it is essential to model the particle–particle interaction at nanoscale accurately in order to understand the overall powder bed and size distribution effect on the selective laser sintering process. Therefore, in order to better understand the parameters that effect void formation in μ-SLS parts, this paper uses discrete element modeling techniques to investigate the role of cohesive forces and particle size distribution on the packing density of nanoparticles in a μ-SLS powder bed.

1.1. Background

Discrete element modeling (DEM) has been a commonly used method for examining the packing and agglomeration of particles in powder systems over the past 30 years. Early DEM based computational models focused on analyzing how microscale particles with uniform size distributions pack together in powders where gravity is the major driving force for packing [9,10]. In these microparticle based systems, cohesive forces such as the van der Waals force do not play a significant role in how particle systems pack together [11]. Instead, the size distribution of particles within the powder system is the most important factor in determining in how the particles pack together in these types of systems [12]. However, in nanoparticle based systems, cohesive forces do play a significant role in the agglomeration and packing of particles within the powder system [13]. Therefore, both cohesive forces as well as particle size distributions need to be considered when analyzing packing in nanoparticle based systems [14].

One of the most common methods for modeling cohesive forces in nanoparticle based systems is to use the Johnson, Kendall, Roberts (JKR) model [15]. In the JKR model of cohesive contact, a balance is created between the elastic energy stored in the particle and the loss in surface energy that is created when two particles are in contact. In the JKR model, only contact pressure and adhesion within the area of contact are considered. This model has been used to examine both how nanoparticles agglomerate and pack together within a powder [16] as well as to model the strength of those agglomerations [17,18].

Cohesive contact is modeled in this paper using an alternative to JKR theory called the Derjaguin-Muller-Toporov (DMT) model [19], which accounts for cohesive forces both within and outside the area of contact between the nanoparticles in order to help accurately model the agglomeration of nanoparticles within the μ-SLS powder bed. The DMT model is used in these simulations because DMT theory has been shown too accurately model metal and ceramic nanoparticle systems, such as the copper nanoparticle system analyzed in this paper [20]. This is because these systems tend to have relatively small and hard particles with low surface energies and, therefore, adhesion in these systems is dominated by weak, long-range attractive forces outside the contact zone [21–23]. In addition, nanoscale asperities on the surface of the nanoparticles can play a significant role in the cohesive forces effecting the nanoparticles [24,25]. Therefore, the DMT contact adhesion model used in this paper has been modified to account for the fact that nanoscale roughness on the surface of the nanoparticle can significantly affect the adhesion forces on the nanoparticles.

In this paper, modified DMT theory is used to examine both how different types of cohesive interactions (none, weak, and strong) and particle size distributions (log-normal, Gaussian, uniform) effect how powder beds form (including packing fraction and density) in microscale selective laser sintering systems. This paper also explores how the presence of a gravitational driving force effects particle packing within a nanoparticle based powder bed system. This includes examining both how all of these parameters effect the agglomeration of nanoparticles as well as the packing of nanoparticles within individual agglomerates. This type of study has not been previously performed in the literature and is very important for designing powder spreader systems for μ-SLS. In addition, the results of this study provide a key motivation for moving from a dry powder spreading mechanism to one involving solvents in nanoparticle based powder bed systems.

2. Modeling approach

The powder bed, consisting of solid, spherical nanoparticles that are generated by defining a position and radius, is created using the discrete element method (DEM) in a multiphase computational fluid dynamics, MFIX. Particle packings are generated using the MFIX-DEM discrete mass inlet function with each particle interacting with its neighboring particles. The particles are initially distributed randomly within the powder bed domain and are given an initial velocity and an initial set of boundary conditions. Forces such as gravitational and cohesive forces are also applied to each particle. Material properties such as diameter, density, and different particle size distribution can also be defined by the user. The MFIX-DEM approach is explained in detail in [26] and summarized briefly below. Our simulation analysis predicts different force analysis contributions such as cohesive and gravitational force within given particle distributions.

2.1. Discrete element method (DEM)

In the discrete element method (DEM), a number of spherical particles, N_m, with diameter, D_m, and density, ρ_{sm} are used to represent the nanoparticle in the powder bed. The total number of particles in the powder bed is given by the summation of each spherical particle over the total number of solid phases, M, as given by Eq. (1).

$$N = \sum_{m=1}^{M} N_m \tag{1}$$

Each of the N particles is defined within a Lagrangian reference at time t by its position, $X^{(i)}(t)$, linear velocity, $V^{(i)}(t)$, angular veloc-

Please cite this article in press as: A. Yuksel, M. Cullinan, Modeling of nanoparticle agglomeration and powder bed formation in microscale selective laser sintering systems, Addit Manuf (2016), http://dx.doi.org/10.1016/j.addma.2016.07.002

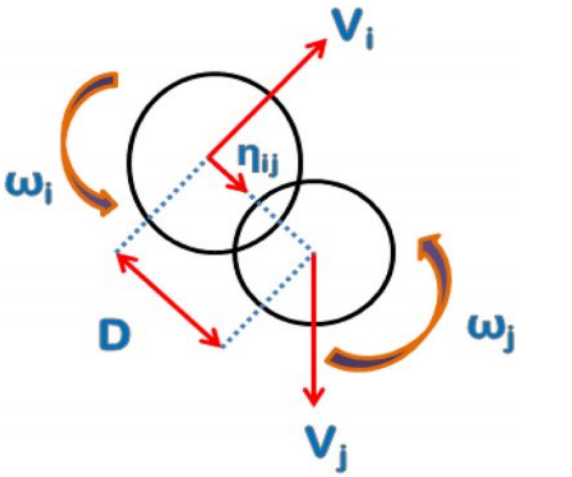

Fig. 1. Schematic of two particles in contact.

ity, $\omega^{(i)}(t)$, diameter, $D^{(i)}$, density $\rho^{(i)}$, and mass $m^{(i)}$. The position, linear velocity and angular velocities of the i^{th} particle change with time according to Newton's laws as below:

$$\frac{dX^{(i)}(t)}{dt} = V^{(i)}(t) \tag{2}$$

$$m(i)\frac{dV^{(i)}(t)}{dt} = F_T(i) = m^{(i)}g + F_d^{(i)}(t) + F_c^{(i)}(t) \tag{3}$$

$$I^{(i)}\frac{d\omega^{(i)}(t)}{dt} = T^{(i)} \tag{4}$$

The total drag force, $F_d(i)$, is found by the summation of pressure and viscous forces. The net contact force, $F_c(i)$, is the force acting on the particle as a result of contact with other particles and the total force on each particle, $F_T^{(i)}$, is found through the summation of all forces acting on the i^{th} particle. Also, the summation of all torques acting on the i^{th} particle is represented by $T^{(i)}$.

2.1.1. Contact forces

A spring-dashpot model, based on a soft-sphere model of the particles, is used for the particle interactions modeled in this study. This model also accounts for the degree of overlapping between two nanoparticles as it imposes no restrictions for multi-particle contacts.

For the soft–sphere collision shown in Fig. 1, two particles, *i* and *j*, in contact have diameters equal to $D^{(i)}$ and $D^{(j)}$, and are located at positions $X^{(i)}$ and $X^{(j)}$ move with linear velocity, V, and an angular velocity, ω. The normal overlap between the particles is given by Eq. (5) and the unit vector along the line of contact between each particle is given by Eq. (6).

$$\delta_n = 0.5\left(D^{(i)} + D^{(j)}\right) - |X^{(i)} + X^{(j)}| \tag{5}$$

$$\eta_{ij} = \frac{\left(D^{(i)} + D^{(j)}\right)}{|X^{(i)} + X^{(j)}|} \tag{6}$$

The relative velocity of the point of contact is given by Eq. (7) where $L^{(i)}$ and $L^{(j)}$ are the distance to the contact point from the center of each particle.

$$V_{ij} = V^{(i)} - V^{(j)} + \left(L^{(i)}\omega^{(i)} + L^{(j)}\omega^{(j)}\right) \times \eta_{ij} \tag{7}$$

For the soft-sphere model used in this paper, the overlap between two adjacent particles is represented by a system of springs and dashpots. The springs are used to model elastic interactions between the particles and the dashpots represent the kinetic energy loss due to inelastic collisions. The springs are given stiffness's in both the normal k_n and tangential, k_t, directions. These stiffness are dependent on the elastic modulus of the nanoparticles that are interacting. Likewise, the dashpot damping coefficients given to each particle interaction in the normal, η_n, and tangential, η_t, directions is determined by the inelastic scattering losses of each nanoparticle collision. Therefore, the normal and tangential components of the contact force, F_{ij}, at time t, can be decomposed into the spring force, F_{ij}^S and the dashpot force, F_{ij}^D, as given by Eqs. (8) and (9).

$$F_{nij}(t) = F_{nij}^S(t) + F_{nij}^D(t) \tag{8}$$

$$F_{tij}(t) = F_{tij}^S(t) + F_{tij}^D(t) \tag{9}$$

The normal spring force, F_{nij}^S, at any time during the contact between two nanoparticles can be calculated using Hooke's law with the displacement equal to the overlap, δ_n, between the particles as shown in Eq. (10).

$$F_{nij}^S = -k_n\delta_n\eta_{ij} \tag{10}$$

Similarly, at any time during the contact, the tangential spring force is given by Eq. (11) where δ_t is the tangential displacement. The tangential displacement at the start of the contact can be calculated as using Eq. (12).

$$F_{tij}^S = -k_t\delta_t \tag{11}$$

$$\delta_t = V_{tij} \times min\left(\frac{|\delta_n|}{V_{ij}\eta_{ij}}, \Delta t\right) \tag{12}$$

For the case of finite Coulomb friction between the particles, then at any time during the contact

$$|F_{tij}^D| > \mu|F_{nij}| \tag{13}$$

where μ is the coefficient of friction. In the case of sliding contact, the tangential dissipative contact force is given by

$$F_{tij}^D = \begin{cases} -\mu|F_{nij}|t_{ij} if t_{ij} \neq 0 \\ -\mu|F_{nij}|\dfrac{\delta_t}{|\delta_t|} if t_{ij} = 0, \delta_t \neq 0 \\ 0 otherwise \end{cases} \tag{14}$$

Therefore, the total tangential force, $F_t^{(i)}(t)$, on the ith particle at any given time and the total torque on the particle, $T^{(i)}(t)$, are given by Eqs. (15) and (16), respectively.

$$F_t^{(i)}(t) = \sum_{j=1}^{N}\left(F_{tij}^S(t) + F_{tij}^D(t)\right) \tag{15}$$

$$T^{(i)}(t) = \sum_{j=1}^{N}\left(L^{(i)}\eta_{ij} \times F_{tij}(t)\right) \tag{16}$$

Overall, the friction component of the tangential force tends to dominate the viscous component in the tangential force calculation for the copper nanoparticle systems studied.

2.1.2. Hertzian model

The linear spring-dashpot model described in the previous section only works well for a small overlap between nanoparticles. For larger overlaps, where the deformation of the nanoparticles is greater than the height of the asperities so that the bulk of the nanoparticle is getting deformed, the linear model must be replaced by a Hertzian contact model [27]. This type of two part stiffness model is necessary because during initial contact, asperities on the surface of the nanoparticle are getting deformed before the bulk of the nanoparticle starts to deform. Therefore, the initial contact stiffness and the bulk stiffness of the nanoparticle can be

Please cite this article in press as: A. Yuksel, M. Cullinan, Modeling of nanoparticle agglomeration and powder bed formation in microscale selective laser sintering systems, Addit Manuf (2016), http://dx.doi.org/10.1016/j.addma.2016.07.002

very different and need to be modeled as two separate stiffnesses [28]. In the Hertzian contact model, the normal and tangential effective spring stiffnesses between two particles in contact can be calculated using the elastic modulus and Poisson's ratio of the nanoparticles as shown in Eqs. (17) and (18) where E_m and E_l are the elastic moduli and σ_m and σ_l are the Poisson ratios for the m^{th} and l^{th} nanoparticles. In addition, G_m, and G_l are the shear moduli of each nanoparticle as calculated by Eqs. (19) and (20), and r_{ml} is the effective contact radius as given by Eq. (21)

$$k_{n,ij} = \frac{4}{3}\frac{E_m E_l \sqrt{r_{ml}}}{E_m\left(1-\sigma_l^2\right)+E_l\left(1-\sigma_m^2\right)}\delta_{n,ij}^{1/2} \tag{17}$$

$$k_{t,ij} = \frac{16}{3}\frac{G_m G_l \sqrt{r_{ml}}}{G_m(2-\sigma_l)+G_l(2-\sigma_m)}\delta_{n,ij}^{1/2} \tag{18}$$

$$G_m = \frac{E_m}{2(1+\sigma_m)} \tag{19}$$

$$G_l = \frac{E_l}{2(1+\sigma_l)} \tag{20}$$

$$\frac{1}{r_{ml}} = \frac{1}{r^{(m)}} + \frac{1}{r^{(l)}} \tag{21}$$

2.1.3. Relationship between dashpot coefficients and coefficients of restitution

The relationship of normal dashpot coefficient η_{nml} and normal coefficient of restitution is given by Eq. (22) where the effective mass (m_{eff}) and collision time (t_{nml}^{col}) between m^{th} and n^{th} solid-phases are defined as $m_{eff} = \left(\frac{m_m m_l}{m_m + m_l}\right)$ and $t_{nml}^{col} = \pi\left(\frac{k_{nml}}{m_{eff}} - \frac{n_{nml}^2}{4m_{eff}^2}\right)^{-1/2}$.

$$\eta_{nml} = \frac{2\sqrt{m_{eff}k_{nml}}|lne_{nml}|}{\sqrt{\pi^2 + lne_{nml}^2}} \tag{22}$$

Time step Δt is taken to be one fiftieth of the minimum collision time (i.e. $\Delta t = \min(t_{col,ml}/50)$). This time step provide sufficient resolution to capture the energy effects of the collision. The normal spring stiffness coefficient is chosen to be $\sim 10^5$ N/m in order to prevent the time step problems due to the complicated definition of spring coefficients in the simulation. By following the Silbert et al. approach [29], the relationship of the tangential spring stiffness coefficient (k_{tml}) and the normal stiffness coefficient (k_n) is defined as $k_{tml} = \frac{2}{5}k_{nml}$. The tangential damping coefficient and the normal damping coefficient is given as $\eta_{tml} = \frac{1}{2}n_{nml}$. Hence, the coefficient of normal restitution matrix and the tangential coefficient of restitution are written as M x M symmetric matrices for M solid-phases shown in (23). As the matrix is symmetric, the top diagonal or lower diagonal values ($M(M\text{-}1)/2$) for normal coefficient of restitution between the particle interactions are set to define the matrix.

$$[e_n] = \begin{bmatrix} e_{n11} & e_{n12}\cdots & e_{n1M} \\ \vdots & \ddots & \vdots \\ e_{nM1} & e_{nM2}\cdots & e_{nMM} \end{bmatrix} \tag{23}$$

2.1.4. Cohesive forces

At the nanoscale, cohesive forces become the dominant force and play an important role on particle interaction. Moreover, the cohesive force becomes very significant at a very short distance and can cause the agglomeration of nanoparticles. Various cohesive force models that predict the interactions between two nanospherical particles have been suggested [6]. However, the initial cohesive models did not consider surface roughness, which plays a key role in the adhesion of nanoparticles [7]. In fact, no real surface is smooth at the submicron level; even polished silicon wafers are rough at sub-nanometer scale [3]. Hence, the adhesion of nanoparticles is of significant importance in nanoscale applications such as semiconductor fabrication and drug delivery. Recently more complex models have been used to explain the sphere–sphere cohesive interaction by including an asperity value which depends on surface roughness [6,7]. Hence, understanding both the roughness and asperity of the surfaces at nanoscale is crucial for modeling the cohesive forces accurately and thus for modeling powder bed formation in microscale selective laser sintering.

The cohesive force interaction between two nanoparticles or between particle and a surface (i.e. the wall of the simulation box) are modeled using the Derjaguin-Muller-Toporov (DMT) model of elastic contact which has been modified to account for surface asperities. In this model, the cohesive forces are calculated using the inner and outer cutoff values of the particle or the wall as given in Eqs. (24) and (25) where A is the Hamaker constant, R is the equivalent radius, r is the separation distance, ϕ is the surface energy, $rp_{innercutoff}$ and $rp_{outercutoff}$ are the inner and outer cutoff cohesive value between particle–particle interaction, and asperity, h, is the general definition of roughness and impurity on the surface. $rp_{innercutoff}$ and $rp_{outercutoff}$ are the inner and outer cutoff value between particle-wall interaction. The surface energy is given by Eq. (26) where D_0 is the cutoff distance and is equal to r for the surface energy in (24) or $r_{innercutoff}$ for the surface energy in (25). For the nanoparticle-to-nanoparticle interactions, if the inner cutoff radius plus the radii of the two particles is less than the distance between the centers of the two particles, L_P, then the cohesive interaction is calculated using Eq. (25). However, if the L_P is greater than this value but less than the outer cutoff radius plus the radii of the two nanoparticles then Eq. (24) is used to calculate the cohesive interaction. If the distance between the two particles is greater than outer cutoff distance than the cohesive interaction between the two particles is assumed to be negligible. Similarly, for wall-nanoparticle interactions, if the inner cutoff radius plus the diameter of the nanoparticle is less than L_P then the cohesive interaction between the particle and the wall is calculated using Eq. (25). However, if the L_P is greater than this value but less than the outer cutoff radius plus the diameter of the nanoparticle then Eq. (24) is used to calculate the cohesive interaction. If the distance between the wall and the particle is greater than outer cutoff distance then the cohesive interaction between the two particles is assumed to be negligible.

$$F = 2\varphi R\left(\left(\frac{h}{h+R}\right) + \frac{1}{\left(1+\frac{h}{r}\right)^2}\right) \tag{24}$$

$$F_{innercutoff} = 2\pi\varphi R\left(\left(\frac{h}{h+R}\right) + \frac{1}{\left(1+\frac{h}{r_{innercutoff}}\right)^2}\right) \tag{25}$$

$$\varphi = \frac{A}{24\pi D_0^2} \tag{26}$$

Typical simulation parameters for each simulation run are given in the table below.

2.2. Nanoparticle size distribution

Particle-size distribution within the powder bed can significantly affect the mechanical and thermal characteristics of the powder bed such as the surface plasmon resonances and excitation enhancement which can significantly change the quality of the process and the overall level of part shrinkage. Most nanoparticle powder beds have a non-uniform particle size distribution since it

Please cite this article in press as: A. Yuksel, M. Cullinan, Modeling of nanoparticle agglomeration and powder bed formation in microscale selective laser sintering systems, Addit Manuf (2016), http://dx.doi.org/10.1016/j.addma.2016.07.002

Table 1
Simulation Parameters.

Parameter	Value
Minimum Inner Cutoff Particle Radius ($rp_{innercutoff}$)	40 nm
Maximum Outer Cutoff Particle Radius ($rp_{outercutoff}$)	500 nm
Surface Asperity Size (h)	5 nm
Wall Inner Cutoff Value ($rw_{innercutoff}$)	1 μm
Wall Outer Cutoff Value ($rw_{innercutoff}$)	5 μm
Particle-to-Particle Spring Constant	10^8 N/m
Particle-to-Wall Spring Constant	10^9 N/m

is almost impossible to obtain a uniform, mono-sized nanoparticle powder bed. Particle size distributions have been analyzed to understand the effect different distribution characteristics such as narrow, broad size and finer, poly-dispersed structures can have on how well particles pack together [8]. The particle size distributions used in this study are explained at the following section.

2.2.1. Gaussian distribution

Gaussian distribution is a very useful probability method especially when the number of random variables is very large. The probability density of the Gaussian distribution is given in Eqs. (27) where μ is the mean or median and σ is the standard deviation of the distribution. The variance can also be defined as σ^2. The Gaussian distribution is non-zero over the region and is symmetric about its median (Tables 1–3).

$$P(x) = \frac{1}{\sigma\sqrt{2\pi}}\left(e^{-\frac{(x-\mu)^2}{2\sigma^2}}\right) \tag{27}$$

The distribution is properly normalized as $\int_{-\infty}^{+\infty} P(x)\,dx = 1$. The cumulative distribution, D(x), function can also be defined as in equation(y) where erf is the so-called error function.

$$D(x) = \int_{-\infty}^{+\infty} P\left(x'\right)dx' = \frac{1}{\sigma\sqrt{2\pi}}\left(e^{-\frac{(x'-\mu)^2}{2\sigma^2}}\right)dx' = \frac{1}{2}\left[1+\mathrm{erf}\left(\frac{x-\mu}{\sigma\sqrt{2}}\right)\right] \tag{28}$$

2.2.2. Log-normal distribution

Log-normal distribution is a continuous distribution whose logarithm has a normal distribution. It is a very common model used in the fields where the boundaries and the threshold of the distribution is estimated or known. Also, it is applied to model continuous random quantities when the distribution is skewed. For example a nanoparticle distribution that has a hard minimum size cutoff at 0 nm but can have some very large particles could be well modeled using the log-normal distribution. The log-normal distribution is given in Eq. (26) where $x \in (0, \infty)$. Also, μ and σ are called the location and the scale parameter, respectively. These parameters can be related with the mean (μ), standard deviation (σ), and variance (ν) of the non-logarithmic values given as in Eq. (29). Also, mean and the median of the distribution can be defined as $\exp\left(\mu+\frac{\sigma^2}{2}\right)$ and $\exp(\mu)$, respectively.

$$\mu = \ln\left(\frac{m}{\sqrt{1+\frac{\nu}{m^2}}}\right), \quad \sigma = \sqrt{\ln\left(1+\frac{\nu}{m^2}\right)} \tag{29}$$

$$P(x) = \frac{1}{\sqrt{2\pi}\sigma x}\exp\left(-\frac{[\ln(x)-\mu]^2}{2\sigma^2}\right) \tag{30}$$

The cumulative distribution, D(x), function can also be defined as in Eq. (31) where erf is the error function.

$$D(x) = \int_{-\infty}^{+\infty} P\left(x'\right)dx' = \frac{1}{\sqrt{2\pi}\sigma x'}\exp\left(-\frac{[\ln(x')-\mu]^2}{2\sigma^2}\right)dx'$$
$$= \frac{1}{2}\left[1+\mathrm{erf}\left(\frac{\ln(x)-\mu}{\sqrt{2}\sigma}\right)\right] \tag{31}$$

2.3. Computational details of particle bed formation

In the particle bed formation algorithm within the MFIX-DEM framework, a nanoparticle with a random size, linear velocity, and angular velocity is initially placed at a random position within a 1 μm^3 box. Another nanoparticle is then placed within the box at a random position with the constraint that the particles do not initially overlap. If the nanoparticle does not overlap with any particle already in the box then the particle stays in the box. However, if there is overlap with an existing particle in the box then the new particle is removed from the system. If 100 particles in a row are not able to be placed into the box due to overlap with existing particles then the box is deemed to be "full" and the simulation stops trying to place new particles into the box. This results in a 1 μm^3, 3-D box that is full of nanoparticles each with a randomly assigned size, position and initial linear and angular velocities. One hundred straight failed insertions of a new particle into the box is used as the cutoff for stopping to try and place more particles into the box because it was found that this cutoff level was the minimum required to keep the change in void fraction to less than uncertainty of the simulation when the minimum number of failed insertions is doubled. Keeping the failed insertion cutoff as low as possible is important because doubling the number of failed insertions approximately doubles the simulation time.

The 1 μm^3 box is also organized such that the only particle-wall interactions that occur happen at the bottom of the box. Periodic boundry conditions are used in the lateral directions so that when a particle moves out of the box in the lateral direction (i.e. through the side walls) it is treated as moving into the opposite side of the box through the periodic boundary. The particle moving into one side of the box has the same properties as the particle moving out of the other side of the box except for the location difference in the periodic direction. For example, when the particle surface exceeds the periodic boundary on one side, the force interactions with the particles near the boundary on the opposite side are taken into account. Similarly, when the center of the particle exceeds the periodic boundary condition it moves to a new position with the same velocity on the other side of the periodic boundary. This type of boundary condition is commonly used to reduce the number of particles required to accurately simulate the packing of particles [30–35]. This periodic boundary condition also allows the simulation to be carried out smoothly because it ensures that energy is conserved within the system.

The size of the particles in the box is determined by randomly selecting the size of each particle using a particle size distribution function. Three different distribution functions were used in this study: (1) a uniform distribution, (2) a Gaussian distribution, and (3) a log-normal distribution. Once the initial particle sizes, positions, velocities and boundary conditions are set, a time step is given

Please cite this article in press as: A. Yuksel, M. Cullinan, Modeling of nanoparticle agglomeration and powder bed formation in microscale selective laser sintering systems, Addit Manuf (2016), http://dx.doi.org/10.1016/j.addma.2016.07.002

Table 2
Hamaker Constants for Various Types of cohesive Interactions.

Cohesive Interaction Case	Particle to Particle Hamaker Constant	Particle to Bottom Wall Hamaker Constant
Strong cohesive Interaction	28.4×10^{-20} J	14×10^{-20} J
Weak cohesive Interaction	10×10^{-20} J	14×10^{-20} J
No cohesive Interaction	0 J	14×10^{-20} J

Table 3
Performed Simulation Data with Particle Size Standard Deviations for Each Case in Nanometers.

Simulation Type	UniformDistribution	GaussianDistribution	Log-NormalDistribution
No cohesive	Std: NA	Std: 25,15,5	Std: 25,15,5
Only Weak cohesive	Std: NA	Std: 25,15,5	Std: 25,15,5
Only Strong cohesive	Std: NA	Std: 25,15,5	Std: 25,15,5
Weak cohesive with gravitational	Std: NA	Std: 25,15,5	Std: 25,15,5
Strong cohesive with gravitational	Std: NA	Std: 25,15,5	Std: 25,15,5

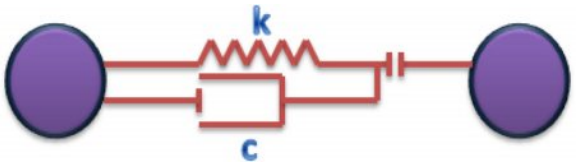

Fig. 2. Schematic of the Spring-dashpot system.

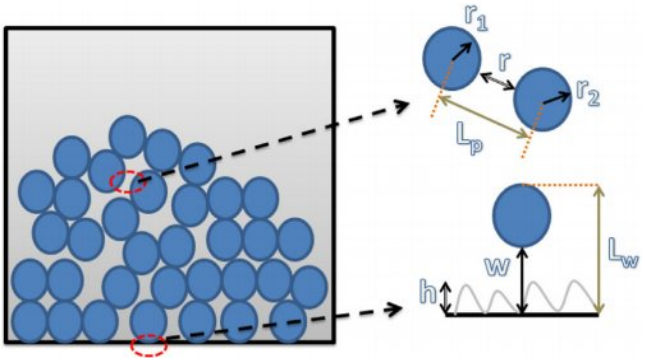

Fig. 3. Schematic view of nanoparticles in the domain. The figure illustrates the following: r is the particle's distance, h is the asperity or surface roughness, w is the separation distance between wall and the particle, L_w and L_p are the distance parameters used for surface-adhesion cohesion.

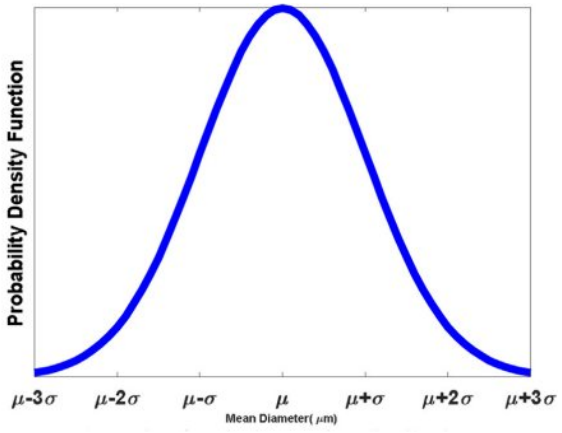

Fig. 4. Schematic of typical Gaussian distribution.

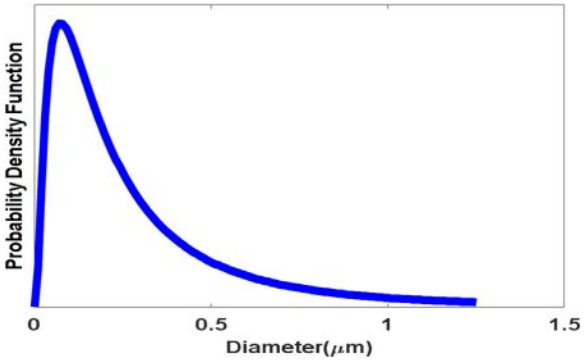

Fig. 5. Schematic of typical log-normal distribution.

to the system and the particles are allowed to move and interact. After the time step, the new position of each particle can be calculated and the interactions between particles can be determined from the overlap between particles. These overlap values determine the forces on each nanoparticle and the amount of energy dissipated by each particle in the time step period. A new set of particle positions, velocities, and boundary conditions can then be determined for the next time step. This process is repeated until the particles reach a steady configuration within the powder bed (Figs. 2–5).

Since the particle bed generation in this paper is random, stochastic process, there will be a slightly varying initial solid fraction between each simulation. This random powder bed generation model is meant to represent the fact that real powder beds will vary in solid fraction when looking at only a small discrete section of the bed. Therefore, in order to understand what is going on in a real powder bed system it is necessary to treat the powder bed generation as a stochastic process. This means that in order to get a good understanding of the powder bed properties, many simulations of the powder bed formation are required in order to determine the average solid fraction, void size, and density in the powder bed as well the typical variance of these parameters. All of the results presented in this paper are averages over a minimum of seven simulations. Overall, the void fraction measured for each case tested was found to be very stable. The typical standard deviation of the seven runs for each case tested was about 3% and the maximum calculated standard deviation found for any case as approximately 5%.

2.3.1. Time integration

A first-order time integration scheme is used to determine the position and the velocity of each particle at each time step. In this scheme, the translational velocity, particle center position, and the angular velocity at time $t + \Delta t$ are obtained from values at time

Please cite this article in press as: A. Yuksel, M. Cullinan, Modeling of nanoparticle agglomeration and powder bed formation in microscale selective laser sintering systems, Addit Manuf (2016), http://dx.doi.org/10.1016/j.addma.2016.07.002

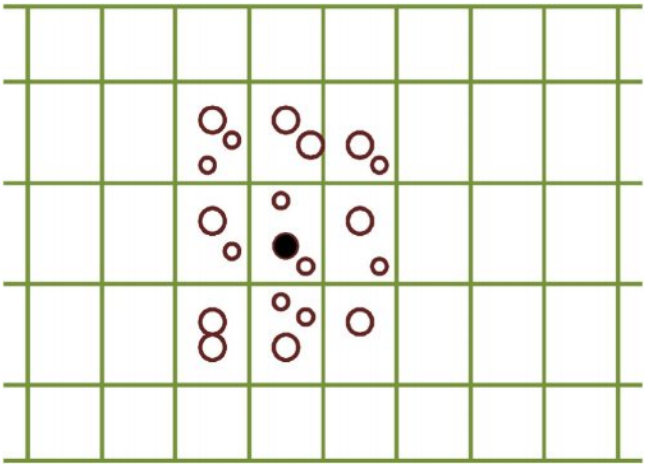

Fig. 6. Neighbor search algorithm for "cell-linked list" in 2D scheme.

t using Eqs. (32)–(34) where $F_T^{(i)}$ and $T^{(i)}$ are the total force and torque acting on the particle.

$$V^{(i)}(t+\Delta t) = V^{(i)}(t) + \frac{F_T^{(i)}(t)}{m^{(i)}}\Delta t \tag{32}$$

$$X^{(i)}(t+\Delta t) = X^{(i)}(t) + V^{(i)}(t+\Delta t)\,\Delta t \tag{33}$$

$$\omega^{(i)}(t+\Delta t) = \omega^{(i)}(t) + \frac{T^{(i)}(t)}{I^{(i)}}\Delta t \tag{34}$$

2.3.2. Neighbor search algorithm

The neighbor search algorithm is one of the most important and time consuming components of any particle–based simulation. Each particle is marked according to the cell in which the center of the particle is located and a "cell–linked list" search algorithm is used to find the particles neighbors. In this algorithm, the simulation is broken down into smaller boxes and only particles within the same box as the particle being investigated or in neighboring boxes are considered. For example, as shown by the 2-D schematic in Fig. 6, if the particle of interest is the one represented by the filled circle, then the particles belonging to the 9 (27 for the 3-D case) adjacent cells, along with particles belonging to the same cell as the particle of interest, are considered as potential neighbors. Thus, only these particles are further checked against the particle of interest for a neighbor contact. By eliminating most of the particles in the box from the search algorithm, the total simulation time is significantly reduced. In this search algorithm, any two particles i and j that are located at $X^{(i)}$ and $X^{(j)}$, and have radii R_i and R_j, are considered neighbors if they satisfy the following condition in Eq. (35) where K is an interaction distance constant.

$$|X^{(i)} - X^{(j)}| < K\left(R_i + R_j\right) \tag{35}$$

This search algorithm can, therefore, be used to determine which particles are touching or overlapping as neighbors. This neighbor search algorithm is run for each time step in order to ensure that the simulation does not miss any possible collision between the particles (Fig. 7).

2.4. Cohesive interactions

Agglomeration of nanoparticles is driven by cohesive interactions between nanoparticles or between a nanoparticle and a surface. For the agglomeration simulations presented in this paper, three general types of cohesive interactions are considered: (1) a strong cohesive interaction case where two dry copper particles interact with each other, (2) a weak cohesive interaction case where the copper nanoparticles are assumed to be encased in a thin polymer or oxide coating, and (3) a no cohesive interaction case where the particles are assumed to be in a perfect colloidal solution. The strength of the cohesive interactions in each case set by adjusting the Hamaker constant of the nanoparticle interaction. In this model, there are assumed to be no cohesive interactions between the top of box and the nanoparticles since in the top layer of the powder bed is open to the environment. Similarly, there are assumed to be no cohesive forces between the sides of the box and the nanoparticles since each box is a discrete element within the continuous powder bed so particles may travel through these boundaries on the side walls. However, there is assumed to be a cohesive interaction between the nanoparticles and the bottom surface of the box since the bottom surface will contain the nanoparticles from the previous sintered layer. The Hamaker constants for each of the cohesive interaction case [36] are given in the table below.

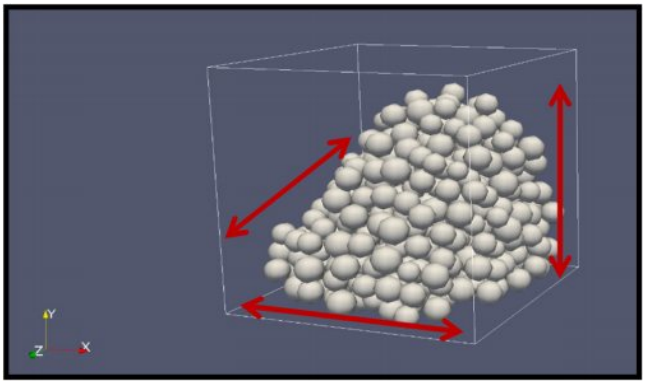

Fig. 7. Typical agglomeration simulation result showing particle clustering into a single portion of the original 1 μm^3 box.

2.5. Particle size distributions

In this study, three different types of particle size distributions were examined: (1) a uniform distribution where all the particles were 100 nm in diameter, (2) a Gaussian distribution with a mean diameter of 100 nm, and (3) a log-normal distribution with a mean diameter of 100 nm. In addition, the Gaussian and log-normal cases were tested with distribution standard deviations of 5 nm, 15 nm, and 25 nm. Limits of 1 nm and 200 nm on the minimum and maximum particle size respectively were also set for both the Gaussian and log-normal distributions. The total number of the particles generated in the 1 μm^3 simulation box for both the Gaussian and log-normal distributions ranged from 263 particles of the 25 nm standard deviation case to 455 for the 5 nm standard deviation case.

2.6. Void fraction analysis

Void fraction is defined as the volume of empty space divided by the volume of space filled by nanoparticles in the powder bed. Void fraction is an important parameter in determining how well particles will sinter together in a selective laser sintering process and in determining the quality of the final part produced. In this study, the void fraction was calculated using two different methods. In the first method (referred to in this paper as method 1), the void fraction is found by considering the highest and lowest particles' positions in the x, y, and z-axis and then creating a box that bounds these particles. These new box bounds are then used to determine the maximum volume that the particles could fill (V_{cube}). This method provides a much better analysis than considering the volume of the whole 1 μm^3 box since the particles will always settle into some subsection of the original box. Once the volume of the bounding

Please cite this article in press as: A. Yuksel, M. Cullinan, Modeling of nanoparticle agglomeration and powder bed formation in microscale selective laser sintering systems, Addit Manuf (2016), http://dx.doi.org/10.1016/j.addma.2016.07.002

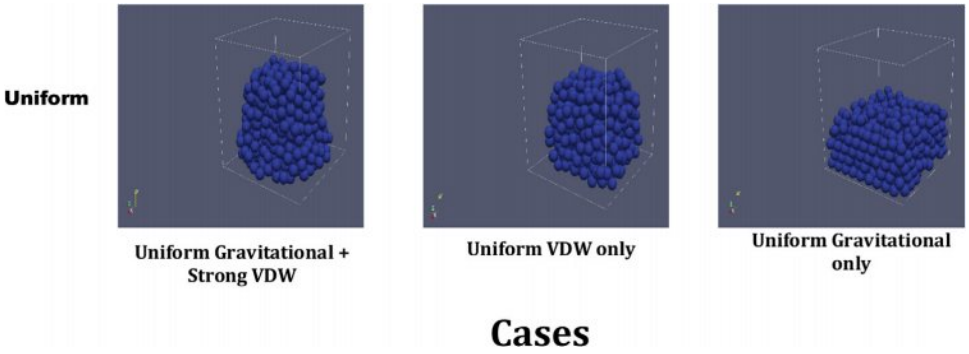

Fig. 8. Simulations with uniform particle distributions and different cohesive force.

box has been found, the void fraction can be found by calculating the volume of all n number of particles in the box and subtracting that volume from the box volume and dividing by the void fraction as shown in Eqs. (36) through (38).

$$\text{Fraction} = \frac{\text{Empty}}{\text{Fill}} \tag{36}$$

$$\text{Empty} = V_{\text{cube}} - \sum_{j=1}^{n} \frac{4}{3}\pi r_j^3 \tag{37}$$

$$V_{\text{cube}} = \left((\max(\text{Position x} + \frac{\text{Diameter}}{2}\right) - \min(\text{Position x} - \frac{\text{Diameter}}{2}\right) \times (\max(\text{Position y} + \frac{\text{Diameter}}{2} - \min(\text{Position y} - \frac{\text{Diameter}}{2}\right) \times (\max\left(\text{Position z} + \frac{\text{Diameter}}{2}\right) - \min\left(\text{Position z} - \frac{\text{Diameter}}{2}\right)\right) \tag{38}$$

The second method (referred to as method 2 in this paper) for calculating the void fraction is very similar to the first except that only the change in the height of the agglomerated cluster in the vertical direction is considered when calculating the bounding box. The extent of the bounding box in the two horizontal directions is set to be the width of the original 1 μm^3 box. This calculation allows us to take into account the effect that clustering of nanoparticles into discrete agglomerates might have on the overall packing density of the nanoparticles in the powder bed. By comparing the void fraction results from each of the two methods it is possible to separate out voids that are created by the packing of the nanoparticles within an agglomerate and the voids that are formed by the agglomeration process itself.

2.7. Test cases

The objective of this study is to quantify and compare the aggregation kinetics and colloidal stability of nanoparticle powder beds with different types of inter-particle interaction forces. In order to pursue that goal the following types of simulations were performed:

3. Results and discussion

3.1. Uniform distribution of particles

Overall, in this study, the uniform distribution of particles will be used as a basis of comparison for evaluating the effect of particle size distribution on the packing quality of the nanoparticles in the μ-SLS powder bed. As can clearly be seen in Fig. 8, cohesive forces (labeled VDW in Figs. 8, 9, and 11 since van der Waals forces are the most significant cohesive force in this model) play a significant role in the agglomeration of particles at the nanoscale. When the only forces applied to the nanoparticle system are gravitational forces, then the particles are able to find their lowest energy state and pack into an ordered cell. However, when cohesive forces are present individual particles adhere together before they can reach their lowest energy state which reduces the packing order. For example, when only gravitational forces are applied to the system the void fraction is approximately 50%. However, when both cohesive and gravitational forces are applied to the system then the void fraction climbs to approximately 65% due to the agglomeration effects created by the cohesive forces. Interestingly, when only cohesive force are considered in the absence of a gravitational driving force, the void fraction is approximately 60%. This reduction in the void fraction in the absence of the gravitational force may be due to the fact the particles take a much longer time to settle into their final positions if there is no global external driving force pushing them towards their final resting position. Therefore, the particle systems without the gravitational force may be able to find a lower energy configuration and better packing than the systems driven by gravitational forces.

3.2. Strong cohesive interaction force case

The effect of particle size distribution on the packing density for a pure copper nanoparticle system can be examined using the strong cohesive force interaction cases. In these types of systems, the smallest particles in the system have the largest cohesive forces on them and, therefore, act as nucleation sites for the formation of agglomerates. In general, the particle distributions with the larger standard deviations pack better (lower void fraction) than the distributions with the smaller standard deviations; however, this is not a strong effect and it can be overwhelmed by random variances do the randomized initial conditions placed on the nanoparticles at the start of the simulation. This general effect can be explained by the fact that with the large particle size standard deviations, there are both more very large and very small nanoparticles that all get packed together. Therefore, the small nanoparticles can generally fill into interstitial spaces between the larger particles in order to increase the overall packing density of the system.

The exception to this trend is the completely uniform distribution which agglomerates in a different way than the distributions with some non-zero standard deviation. In even the distributions with the narrowest standard deviations, there are occasionally small particles that can act like a nucleation site to form agglomeration which results in a heterogeneous type nucleation of the agglomerate. However, in the uniform distribution, there are no small particles to act as a preferential nucleation site. This results

Please cite this article in press as: A. Yuksel, M. Cullinan, Modeling of nanoparticle agglomeration and powder bed formation in microscale selective laser sintering systems, Addit Manuf (2016), http://dx.doi.org/10.1016/j.addma.2016.07.002

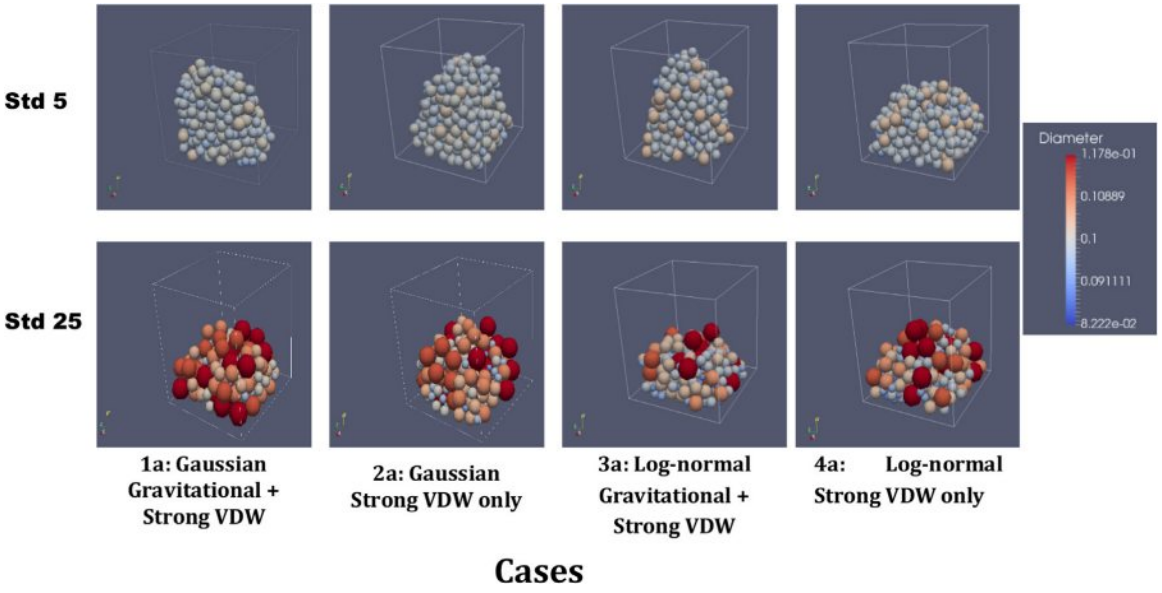

Fig. 9. Images of nanoparticle agglomeration for 4 different strong cohesive cases with particle size standard deviations of 5 nm and 25 nm.

in homogeneous nucleation of the agglomerate in the uniform distribution case. As a result of this homogeneous nucleation, the uniform distribution tends to have a better packing density than either the small standard deviation Gaussian or log-normal distribution cases. This indicates that it may be the smallest particles in the powder distribution that most effect agglomeration and not the overall uniformity or size distribution of the nanoparticles. Therefore, one strategy to reduce agglomeration would be to eliminate all of the very small particles from the powder bed. However, in practice it may be impossible to create particle distributions without any small particles that can act as nucleation sites. Overall, the results of these simulations show that it is important to be able to measure and evaluate the size distributions of the nanoparticles in a μ-SLS powder bed in order to evaluate the effect these nucleation sites will have on void formation.

In addition, as can be seen in Fig. 10, the void fraction calculated using method 1 in Section 2.5 is always smaller than or equal to the void fraction calculated using method 2 where the entire width of the initial bounding box is considered in the calculation. This makes sense because the horizontal extent of the nanoparticles will always be smaller than or equal to the original 1 μm^3 bounding box. Therefore, the ratio of these two void calculation methods can be used as a proxy for the extent of agglomeration in the nanoparticle system and can be used to separate the effect of packing voids from voids caused by agglomeration. The error bars in Figs. 10, 12, and 14 represent the standard deviation of the calculated void fraction over all the trials simulated for that case and distribution.

3.3. Weak cohesive interaction case

Cohesive interactions between nanoparticles can be reduced by coating the copper nanoparticles with a thin oxide or polymer coating. This reduction in the cohesive forces means that only the very smallest nanoparticles produce a high enough adhesion force to act as nucleation sites for agglomeration. Therefore, there are fewer nucleation sites in the weak cohesive case than there were in the strong cohesive case. Because of these fewer number of nucleation sites, the nanoparticles tend to agglomerate into columnar-like crystals as can be clearly seen for the Gaussian, weak cohesive force case (2b) with a particle size standard deviation of 5 nm as shown in Fig. 11.

This produces a relatively efficient packing of the particles within the agglomerate (similar to the strong cohesive case) but does increase the overall agglomerate size. This is because the lower number of nucleation sites in the weak cohesive case cause the agglomerate to generally form from a single nucleation site in the simulation instead of multiple nucleation sites as is the case with the strong cohesive case. This result can be seen when the void fraction is calculated using method 2 in Section 2.5. Overall, when the void fractions are calculated for the weak cohesive case using

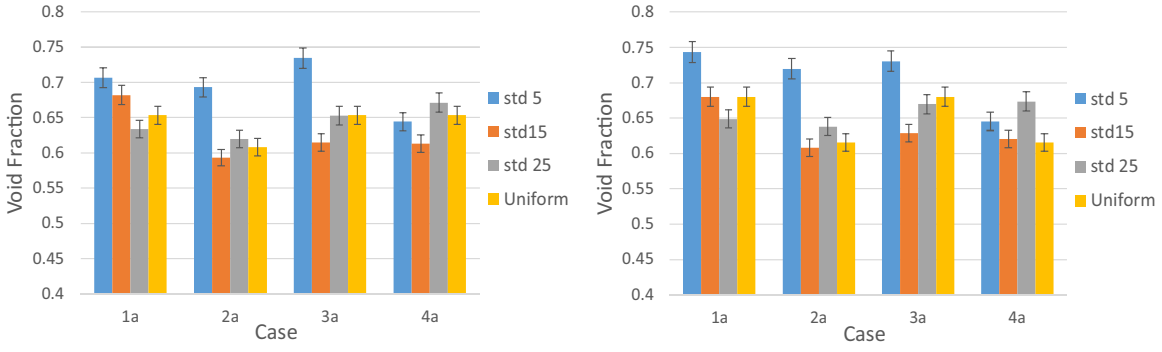

Fig. 10. For Strong cohesive interactions: (Left) Void fraction calculated based on particle's x,y and z direction i.e method 1 (right) Void fraction calculated based on particle's y direction only (x = z = 1 μm) i.e. method 2.

Please cite this article in press as: A. Yuksel, M. Cullinan, Modeling of nanoparticle agglomeration and powder bed formation in microscale selective laser sintering systems, Addit Manuf (2016), http://dx.doi.org/10.1016/j.addma.2016.07.002

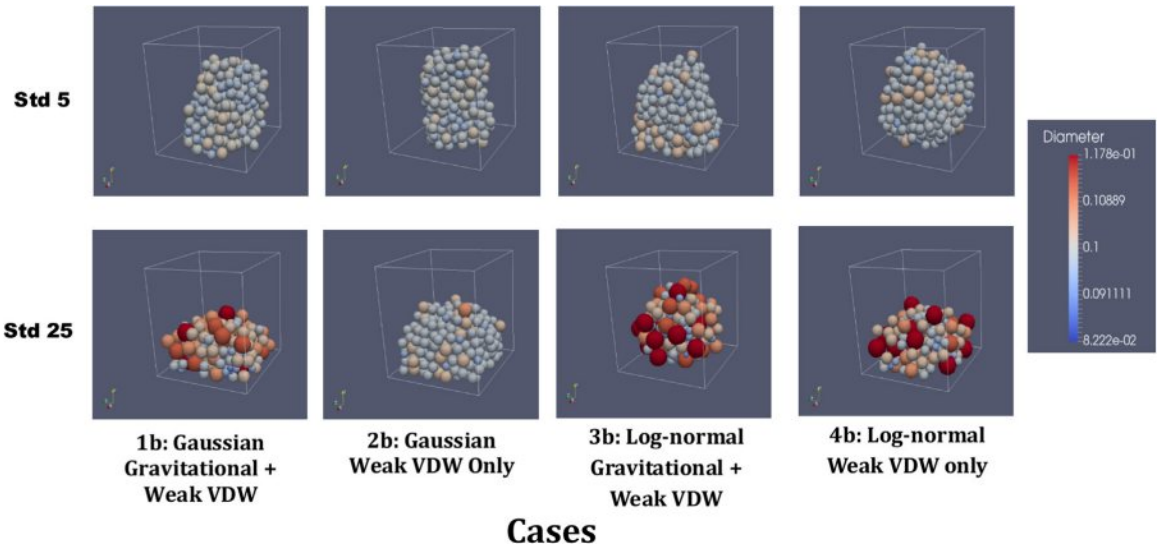

Fig. 11. Images of nanoparticle agglomeration for 4 different weak cohesive cases with particle size standard deviations of 5 nm and 25 nm.

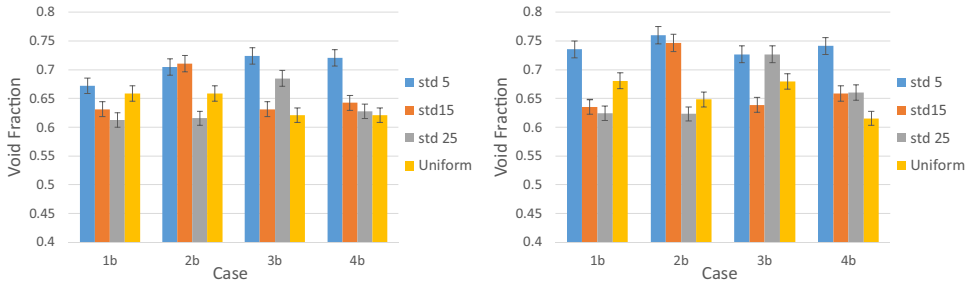

Fig. 12. For weak cohesive interactions: (Left) Void fraction calculated based on particle's x,y and z direction i.e method 1 (right) Void fraction calculated based on particle's y direction only (x = z = 1 μm) i.e. method 2.

method 1 they are not significantly different from the void fractions calculated in the strong cohesive case. However, when the void fractions are calculated using method 2, the weak cohesive cases produce void fractions that are about 10% larger than those that were produced in strong cohesive case. This suggests that just reducing the cohesive interactions between the nanoparticles alone may not be enough to reduce agglomeration in μ-SLS powder beds.

3.4. No cohesive (gravitational only) case

One potential method to reduce agglomeration in μ-SLS powder beds is to dispense the powder in a liquid as a colloidal solution and then to coat the solution into a uniform layer. This layer can then be allowed to dry in order to produce the new μ-SLS powder bed layer. The advantage of this method is that while the particles are in the colloidal solution, surfactants can be used to effectively eliminate cohesive interactions between the particles. The simulation results indicate that the presence of cohesive interactions within the powder bed can cause the void fraction in the particle agglomerates to increase by up to 34% for the low standard deviation, Gaussian case and by up to 40% in the low standard deviation, log-normal distribution case.

In addition, the elimination of the cohesive interactions eliminates the large scale formation of agglomeration within the μ-SLS powder bed. This can be seen by the fact that when the void density is calculated using each of the two methods presented in Section 2.5, both methods produce the exact same results. Therefore, the two bar charts created using each of the two void fraction calculation methods in Fig. 14 are identical. This indicates that the particles are spreading out to the edges of the initial bounding box, as can be seen in Fig. 13, so that they can form continuous nanoparticle layers. Therefore, one of the key to producing good, uniform sintering layers in μ-SLS powder beds is to eliminate the cohesive interactions between the nanoparticles in the powder beds.

4. Comparison to experimental results

In order to validate the predictions made by the simulations presented in the previous section, several nanoparticle surface spreading experiments were performed. First, 100 nm diameter average size copper nanoparticles from various commercial venders (US Research Nano and MK Impex) were spread onto glass slides and silicon substrates. As shown in Fig. 15, these nanoparticles tended to agglomerate into very large, discrete assemblies. These agglomerated particles assemblies can be on the order of 100 μm in diameter and can consist of hundreds of thousands of nanoparticles. These agglomerates contain many more particles than it is possible to simulate using the discrete element method, but the results from the DEM simulations do show very similar agglomeration formation within the smaller simulation volume for both the strong and weak cohesive cases. In addition, samples passivated with oxide, carbon, and polymer coatings were tested to see how much agglomeration takes place in powder beds generated using these types of passivated particles. The passivation coatings are meant of reduce agglomeration the nanoparticles when they are in powder form by reducing the cohesive interactions between the particles. However, even with the passivated coatings, significant agglomeration of the nanoparticles was observed. This observed

Please cite this article in press as: A. Yuksel, M. Cullinan, Modeling of nanoparticle agglomeration and powder bed formation in microscale selective laser sintering systems, Addit Manuf (2016), http://dx.doi.org/10.1016/j.addma.2016.07.002

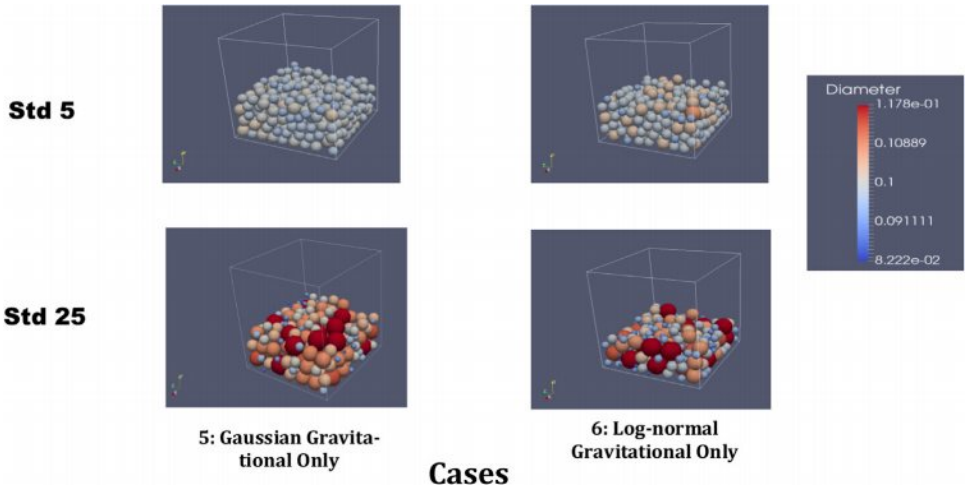

Fig. 13. Images of nanoparticle agglomeration for 2 different no cohesive cases with particle size standard deviations of 5 nm and 25 nm.

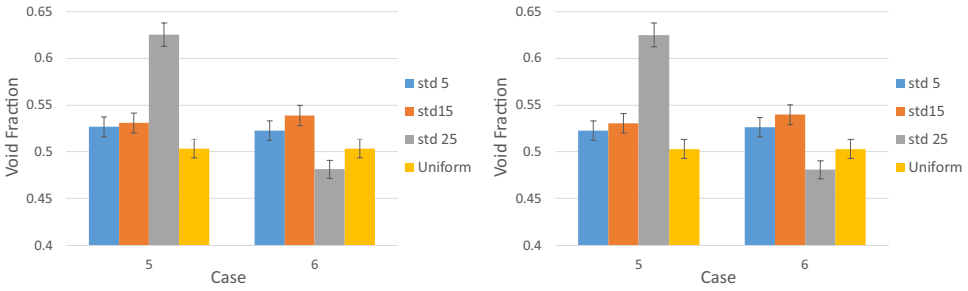

Fig. 14. For gravitational forces only: (Left) Void fraction calculated based on particle's x,y and z direction i.e. method 1 (right) Void fraction calculated based on particle's y direction only (x = z = 1 μm) i.e method 2.

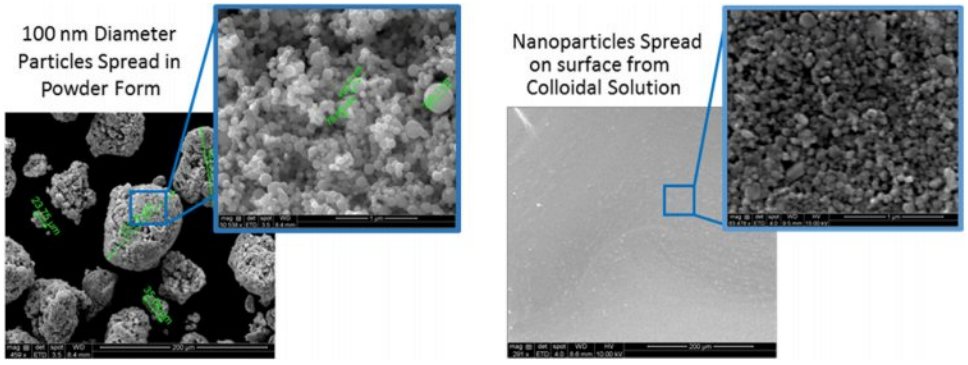

Fig. 15. (Left) Agglomeration of ~100 nm diameter nanoparticles in powder form (Right) ~100 nm diameter nanoparticles spread onto surface and dried showing no agglomeration of particles.

result matches very well what the discrete element model simulations for the weak cohesive case predict. This indicates that the simulations that include non-zero cohesive interactions do a good job predicting nanoparticle agglomeration in the μ-SLS powder bed.

One potential method to overcome the agglomeration effects due to cohesive interactions is to dispense the nanoparticles as part of a colloidal solution and then to dry the solution to form the powder layer. In order to test this method, a commercially available colloidal solution of copper nanoparticles (Applied Nanotech) was spin coated onto a silicon substrate and was dried on a hotplate. As can be seen in Fig. 15, this method of spreading the copper nanoparticles produces a much more continuous and uniform nanoparticle layer than the powder spreading method. This result matches well with the predictions made by the no cohesive force discrete element simulation models. Overall, based on this result, it may be possible to create much more uniform nanoparticle beds for μ-SLS using a solution-based deposition method such as spin coating or slot-die coating than by using more traditional powder spreading methods, such as the use of a counter-rotating roller or a doctor blade to spread a dry powder, which are commonly used in larger scale SLS operations.

5. Conclusions

In this paper, a particle–particle interaction model was used to generate a random packing of nanoparticles and an analysis of the packing fraction of Cu nanoparticles of given particle size

Please cite this article in press as: A. Yuksel, M. Cullinan, Modeling of nanoparticle agglomeration and powder bed formation in microscale selective laser sintering systems, Addit Manuf (2016), http://dx.doi.org/10.1016/j.addma.2016.07.002

distribution by means of MFIX-DEM simulations was presented. In this study, nanoparticles were injected into the domain from the top boundary and allowed to fall under the influence of gravity and cohesive forces. Once the particles settle, their positions and properties are can be used as an input for the optical model. The extinction and effective absorption coefficient of a powder bed hence can be calculated. The simulations were done for different cases such as for pure copper nanoparticles, copper nanoparticles with a polymer or oxide coating, and copper nanoparticle in a colloidal coating. The coatings and treatments of the nanoparticles can significantly affect the cohesive interactions between particles. The effects of various types of particle size distributions (uniform, Gaussian, and log-normal) were also studied for different standard deviations. The particles in the simulation are assumed to not initially overlap and to not initially be deformed due to the adhesion or contact effects. The simulations are run until all particles settle on the surface and find their final resting position. Contact forces are obtained by Newton's laws based on the position, the linear, and the angular velocities of each of the individual particles in the simulation. A spring-dashpot model is used for particle interactions between the nanoparticles and between the nanoparticles and the walls of the simulation. The simulation takes an average time of $3*10^5$ seconds on an Intel 8-Core Xeon Processor.

Overall, these simulations show that cohesive forces have a significant influence on how nanoparticles agglomerate within the μ-SLS powder bed. Nanoparticles subject to strong cohesive forces agglomerate very rapidly with multiple nucleation points. This leads to non-optimal packing densities but relatively small agglomerates. Nanoparticles subject to weaker cohesive forces still form agglomerates but the agglomerated assemblies are generally larger and take longer to form than in the strong cohesive case due to the lower number of potential agglomeration nucleation sites. When cohesive interactions between the nanoparticles are eliminated, such as in a colloidal suspension of nanoparticles, the nanoparticles are able to form densely packed, continuous nanoparticle layers as opposed to discrete agglomerated particle assemblies. This result suggest a new potential method for creating nanoparticle layers in μ-SLS additive manufacturing systems using colloidal solutions. However, more work still needs to be done to determine how well nanoparticles deposited from colloidal solutions can be sintered together and to determine what effect residual surfactants from the colloidal suspension might have on the quality of the final sintered part.

Acknowledgement

The authors would like acknowledge Prof. Jayathi Murthy and Daniel Moser for their guidance and valuable contributions. We would like to thank Nilabh Roy for providing the SEM pictures and comments on experimental analysis. The authors would like to acknowledge CS Foong and Leo M. Higgins from NXP Inc. for their helpful comments and suggestions.

References

[1] T. Sun, J. Wang, W. Kang, van der Waals interaction-tuned heat transfer in nanostructures, Nanoscale 5 (2013) 128–133.
[2] O. Ivanova, C. Williams, T. Campbell, Additive manufacturing (AM) and nanotechnology: promises and challenges, Rapid Prototyp. J. 19 (5) (2013) 353–364.
[3] Y. Samitsu, Nanotechnology 4 (1993) 236.
[4] Y. Mo, K. Turner, I. Szlufarska, Friction laws at the nanoscale, Nature 457 (2009) 1116–1119.
[5] W. Sun, Interaction forces between a spherical nanoparticle and a flat surface, Phys. Chem. Chem. Phys. 16 (2014) 5846–5854.
[6] Q. Li, V. Rudolph, W. Peukert, London-van der Waals adhesiveness of rough particles, Powder Technol. 161 (2006) 248–255.
[7] J. Katainen, M. Paajanen, E. Ahtola, V. Pore, J. Lahtinen, Adhesion as an interplay between particle size and surface roughness, J. Colloid Interface Sci. 304 (2006) 524–529.
[8] J. Ma, L. Lim, Effect of particle size distribution on sintering of agglomerate-free submicron alumina powder compacts, J. Eur. Ceram. Soc. 22 (13) (2002) 2197–2208.
[9] K.Z.Y. Yen, T.K. Chaki, A dynamic simulation of particle rearrangement in powder packings with realistic interactions, J. Appl. Phys. 71 (7) (1992) 3164–3173.
[10] R.Y. Yang, R.P. Zou, A.B. Yu, Computer simulation of the packing of fine particles, Phys. Rev. E 62 (3) (2000) 3900.
[11] R. Tayeb, X. Dou, Y. Mao, Y. Zhang, Analysis of cohesive microsized particle packing structure using history-dependent contact models, J. Manuf. Sci. Eng. 138 (4) (2016) 041005.
[12] Eric J.R. Parteli, et al., Attractive particle interaction forces and packing density of fine glass powders, Sci. Rep. 4 (2014).
[13] R. Moreno-Atanasio, S.J. Antony, R.A. Williams, Influence of interparticle interactions on the kinetics of self-assembly and mechanical strength of nanoparticulate aggregates, Particuology 7 (2) (2009) 106–113.
[14] Z. Peng, E. Doroodchi, G.M. Evans, Influence of primary particle size distribution on nanoparticles aggregation and suspension yield stress: a theoretical study, Powder Technol. 223 (2012) 3–11.
[15] K.L. Johnson, K. Kendall, A.D. Roberts, Proc. R. Soc. Lond. A 324 (1971) 301.
[16] Xiaoliang Deng, James V. Scicolone, Rajesh N. Davíe, Discrete element method simulation of cohesive particles mixing under magnetically assisted impaction, Powder Technol. 243 (2013) 96–109, http://dx.doi.org/10.1016/j.powtec.2013.03.043, ISSN: 0032-5910.
[17] C. Thornton, M.T. Ciomocos, M.J. Adams, Numerical simulations of diametrical compression tests on agglomerates, Powder Technol. 140 (2004) 258–267, http://dx.doi.org/10.1016/j.powtec.2004.01.022.
[18] K.D. Kafui, C. Thornton, Numerical simulations of impact breakage of a spherical crystalline agglomerate, Powder Technol. 109 (1–3) (2000) 113–132, http://dx.doi.org/10.1016/S0032-5910(99)00231-4, ISSN: 00325910.
[19] B.V. Derjaguin, V.M. Muller, Y.P. Toporov, J. Colloid Interface Sci. 53 (1975) 314.
[20] R. Jasevivius, P. Baltrenas, R. Kacianaukas, G. Raimondas, DEM simulation of the impact of ultrafine glass particles on the partition wall of the multichannel cyclone, Part. Sci. Technol. 32 (2014) 576–587.
[21] D.S. Grierson, E.E. Flater, R.W. Carpick, Accounting for the JKR—DMT transition in adhesion and friction measurements with atomic force microscopy, J. Adhes. Sci. Technol. 19 (3) (2005) 291–311.
[22] D. Guo, G. Xie, J. Luo, Mechanical properties of nanoparticles: basics and applications, J. Phys. D Appl. Phys 47 (2014) 013001.
[23] X. Shi, Y. Zhao, Comparison of various adhesion contact theories and the in uence of dimensionless load parameter, J. Adhes. Sci. Technol. 18 (1) (2004) 55–68.
[24] O. Laitinen, et al., Validity of the Rumpf and the Rabinovich adhesion force models for alumina substrates with nanoscale roughness, Powder Technol. 246 (2013) 545–552.
[25] Kevin Cooper, Anand Gupta, Stephen Beaudoin, Simulation of the adhesion of particles to surfaces, J. Colloid Interface Sci. 234 (2) (2001) 284–292.
[26] R. Garg, J. Galvin, T. Li, S. Pannala, Documentation of open-source MFIX–DEM software for gas-solids flows (2012).
[27] H. Hertz, Uber die beruhrung fester elastischer korper, (on the contact of elastic solids), J. Angew. Math. 94 (1882) 156–171.
[28] O.I. Imole, D. Krijgsman, T. Weinhart, V. Magnanimo, B.E. Chávez, M. Ramaioli, S. Luding, Experiments and discrete element simulation of the dosing of cohesive powders in a simplified geometry, Powder Technol. 287 (2016) 108–120.
[29] Leonardo E. Silbert, Deniz Ertaş, Gary S. Grest, Thomas C. Halsey, Dov Levine, Steven J. Plimpton, Granular flow down an inclined plane: bagnold scaling and rheology, Phys. Rev. E 64 (2001) 051302.
[30] W. Yang, Z. Zhou, D. Pinson, A. Yu, Periodic boundary conditions for discrete element method simulation of particle flow in cylindrical vessels, Ind. Eng. Chem. Res. 53 (2014) 8245–8256.
[31] A. Dziugys, B. Peters, An approach to simulate the motion of spherical and non-spherical fuel particles in combustion chambers, Granul. Matter 3 (2001) 231–265.
[32] D.C. Rapaport, The event scheduling problem D. C. in molecular, J. Comput. Phys. 34 (1980) 184–201.
[33] F. Radjai, C. Voivret, Periodic boundary conditions, in: F. Radjai, F. Dubois (Eds.), Discrete Numerical Modeling of Granular Materials, Weiley, 2011, pp. 181–198.
[34] J.R. Third, D.M. Scott, S.A. Scott, C.R. Muller, Effect of periodic boundary conditions on granular motion in horizontal rotating cylinders modelled using the DEM, Granul. Matter 13 (2011) 75–78.
[35] S.B. Kuang, K. Li, R.P. Zou, R.H. Pan, A.B. Yu, Application of periodic boundary conditions to CFD-DEM simulation of gas—solid flow in pneumatic conveying, Chem. Eng. Sci. 93 (2013) 214–228.
[36] I.D. Morrison, S. Ross, Colloidal Dispersions: Suspensions, Emulsions, and Foams, Wiley-Interscience, New York, 2002.

Please cite this article in press as: A. Yuksel, M. Cullinan, Modeling of nanoparticle agglomeration and powder bed formation in microscale selective laser sintering systems, Addit Manuf (2016), http://dx.doi.org/10.1016/j.addma.2016.07.002